

## Article

# 2D-Perovskite Multiferroics: Interface-Induced Magnetoelectric Effect in Perovskite-Based Multiferroic Superlattices

Zukhra Gareeva <sup>1,2,\*</sup> , Ildus Sharafullin <sup>2</sup>  and Anatoly Zvezdin <sup>3,4,\*</sup>

<sup>1</sup> Institute of Molecule and Crystal Physics, Subdivision of the Ufa Federal Research Centre of the Russian Academy of Sciences, 450075 Ufa, Russia

<sup>2</sup> Physico-Technical Institute, Ufa University of Science and Technology, 450076 Ufa, Russia; sharafullinif@yandex.ru

<sup>3</sup> Prokhorov General Physics Institute of the Russian Academy of Sciences, 119991 Moscow, Russia

<sup>4</sup> “New Spintronic Technologies” Limited Liability Company, 121205 Moscow, Russia

\* Correspondence: zukhrazv@yandex.ru (Z.G.); zvezdin@gmail.com (A.Z.)

**Abstract:** Multiferroics are materials crucial for energy-efficient scalable electronics. The implementation of an effective combination of ferroic orderings on the nanoscale requires the design of new multiferroic materials. Recently, there have been observations of magnetoelectricity in the antiferromagnetic Ruddlesden-Popper and perovskite oxides with the interfacial Dzyaloshinskii-Moriya interaction. We propose a model for studying magnetic states and magnetoelectric effects in magnetoelectrically coupled antiferromagnetic–ferroelectric bi-layers with the interfacial Dzyaloshinskii-Moriya interaction. The ground magnetic states are calculated for a system on a rectangular lattice, with Heisenberg spins interacting with each other via an antiferromagnetic exchange interaction and a Dzyaloshinskii-Moriya interaction in the absence of an external magnetic field. Our calculations show that the interfacial Dzyaloshinskii-Moriya interaction in the considered system leads to the stabilization of topological skyrmionic states in a zero magnetic field. We explore transformations of magnetic states considering the changes in the in-plane magnetic anisotropy constant and the magnetoelectric coupling parameter. Our findings have shown the possibility of the existence of several magnetic configurations: a skyrmion lattice, a skyrmion state, and a uniform antiferromagnetic ordering realized at a definite ratio of the system parameters. We determine the areas of the phases existence and the conditions required for spin-reorientation phase transitions.

**Keywords:** magnetoelectric effect; perovskite; Dzyaloshinskii–Moriya interaction; skyrmion



**Citation:** Gareeva, Z.; Sharafullin, I.; Zvezdin, A. 2D-Perovskite Multiferroics: Interface-Induced Magnetoelectric Effect in Perovskite-Based Multiferroic Superlattices. *Crystals* **2023**, *13*, 1404. <https://doi.org/10.3390/cryst13091404>

Academic Editors: Karuna Kara Mishra and Venkata Sreenivas Puli

Received: 29 August 2023  
Revised: 15 September 2023  
Accepted: 17 September 2023  
Published: 21 September 2023



**Copyright:** © 2023 by the authors. Licensee MDPI, Basel, Switzerland. This article is an open access article distributed under the terms and conditions of the Creative Commons Attribution (CC BY) license (<https://creativecommons.org/licenses/by/4.0/>).

## 1. Introduction

The development of energy-efficient electronics requires advanced scalable materials to manipulate robust magnetic states in order to encrypt and process information. In this regard, promising prospects are associated with the class of correlated oxides, in which an abundance of physical phenomena, such as ferroelectricity, multiferroicity, and superconductivity, emerge due to a wide range of crystal structures and related functionalities. A bright example is  $ABO_3$  perovskites, which can crystallize in cubic, orthorhombic, rhombohedral, or hexagonal phases; this type of the syngony is related to the value of the Goldschmidt tolerance factor. Since the realization of certain physical properties depends on the crystallographic symmetry, the structural diversity of  $ABO_3$  perovskites provides a variety of fascinating physical effects, and particular attention is paid to magnetoelectricity and topological defects, due to their demand in spintronics and information storage technologies. It is of importance that both of these phenomena are allowed in crystals with broken spatial inversion symmetry.

Magnetoelectricity attracts a lot of attention, since its implementation in spintronic devices provides ultra-low power consumption. For example, estimations of the energy dissipation per unit area per voltage-induced switch in MF heterostructures give the values

1–500  $\mu\text{J cm}^{-2}$ , which is ten times lower than the energy losses in magnetization reversal processes induced by electric current. The efficiency of the transduction of electric and magnetic energies in magnetoelectric (ME) materials depends on a number of factors, among which the most important are the ME strength and ME response. ME strength is related to the coupling between magnetic and ferroelectric orderings and mostly depends on the intrinsic properties of a system. ME response is determined as the reaction of a magnetic or ferroelectric subsystem to external agents, such as electric voltage or magnetic field. These properties unified in the magnetoelectric coupling coefficient are most pronounced in thin film multilayered heterostructures [1]. The ME coefficient is governed by various interactions and mechanisms (exchange, strain, ionic, and charge [2]), the manifestation of which depends on the composition of the layers and the couplings between them. For example, in ferromagnetic-piezoelectric heterostructure, the predominant ME mechanisms are related to striction effects and strains; in multiferroic-ferromagnetic composites, the main ME contribution is given by exchange bias effects; the ME properties of antiferromagnetic-piezoelectric heterostructures are attributed to the exchange striction induced by the strains. However, despite the variety of possible ME heterostructures and the mechanisms implemented in them, there is still no unified recipe for creating an optimum structure with the efficient ME coefficient ( $\alpha$ ). The  $\alpha$  values seem to be more or less comparable, and the choice of composites is often related to other physical priorities.

Advances in oxide interface technology are expanding the ability to realize various couplings between spin, charge, and lattice excitations [3,4]. In particular, oxide interfaces make it possible to study the spin–orbit interactions, including the Dzyaloshinskii–Moriya interactions (DMI), which can manifest themselves both in the ME effect and the emergence of non-trivial topological structures. Interest in the study of the DMI, renewed in the latest decade due to the discovery of whirling topological structures in non-centrosymmetric magnetic crystals and films, is now penetrating into the magnetoelectric field of research. The DMI in its general form is described by the Lifshitz invariant allowed in the systems with broken inversion symmetry. It stabilizes chiral magnetic structures—cycloids, spirals, 2D vortices, skyrmions, and 3D hopfions—affects the spin dynamics, and gives impact to magnetoelectricity. Magnetoelectric effect in improper multiferroics is mainly attributed to DMI; however, the physical mechanisms, such as DMI-induced polarization of electronic orbitals [5], ferroelectric lattice displacements [6], and the stabilization of incommensurate spin structures, which, in its turn, hosts ferroelectricity [7], are still under discussion. Nevertheless, the existing relationship between the ME effect and DMI allows for the expectation that correct implementation of DMI in multiferroic heterostructures can lead to an improvement in magnetoelectric properties.

The rapidly developing field of strain engineering opens new routes for the design of oxide interfaces and stacked multilayered structures [3,5,8–12]. Much of the current research focuses on the creating and manipulating skyrmion-like states in heterostructures consisting of ferromagnets (FM), antiferromagnets (AFM), and multiferroics (MF) [3,13,14]. Skyrmionic textures recently have been found in a number of multiferroic oxides and heterostructures. The particular examples are mixed-valence manganites ( $\text{Ca}_{1-x}\text{Ce}_x\text{MnO}_3$ ) and manganite films ( $\text{LaMnO}_3/\text{SrIrO}_3$ ) [15], measurements of Hall effects, which revealed the presence of topological skyrmion-like structures,  $\text{SrRuO}_3$ -based heterostructures [10], and ferrimagnetic insulator films, such as iron garnet (YIG, TmIG, TbIG) (see [3] and references therein). The advantage of oxide interfaces is that a low-energy voltage approach can be used to manipulate magnetic states.

Interestingly, the ME effect is rather well manifested in perovskite-based stacked multilayers; this may be due to the oxygen octahedra rotations, which contribute to both ferroelectricity and DMI. Examples to consider include  $\text{BiFeO}_3/\text{SrRuO}_3$ , studied in Ref. [7] and  $\text{Sr}_2\text{IrO}_4/\text{SrTiO}_3$  or  $\text{Sr}_2\text{IrO}_4/\text{BaTiO}_3$  superlattices, studied in Ref. [16]. The advantage of using the Ruddlesden-Popper structures ( $\text{Sr}_2\text{IrO}_4$  for example) as the MF superstructure component is related to the possibility of realizing high-temperature ferroelectricity. The emergence of the magnetoelectric effect and new topological structures in superlattices

consisting of an Ruddlesden-Popper structure and a ferroelectric/paraelectric perovskite substrate due to the interfacial DMI is reported in Ref. [16]. The research focuses on the experimental observations of magnetoelectric phase transitions and concomitant anomalies; however, the theoretical explanation of the phenomena is still lacking.

In this article, we propose a model to describe the possible couplings in layered systems, calculate ground magnetic states, and analyze their transformations, accounting for magnetoelectric effect and the DMI allowed by the symmetry of the considered interface.

The paper is organized as follows. Section 1 contains a brief introduction to R-P structures and symmetry analysis of magnetoelectric couplings in R-P-like structures, Section 2 considers DMI and magnetoelectricity, Section 3 presents calculations of the ground magnetic state in a bi-layered AFM-ferroelectric structure with interfacial DMI. Discussion of the results and concluding remarks are given in Section 4.

## 2. Materials and Methods

### 2.1. Ruddlesden-Popper Structures. Layered Perovskites

Currently, layered perovskites are considered promising candidates for multiferroics due to the possibility of high-temperature magnetoelectric orderings and high values of magnetization [12,17]. Interesting examples include insulators  $\text{Ca}_3(\text{Ti}_{1-x}\text{Mn}_x)_2\text{O}_7$  [18], Mott-insulators  $\text{Sr}_2\text{IrO}_4$  [16,17] and metals  $\text{Bi}_5\text{Mn}_5\text{O}_{17}$  [17], where the manifestation of magnetoelectric properties have been detected. Here, we will focus on the Ruddlesden-Popper (RP) structures with magnetic ions, considering as the examples classical  $\text{Ca}_3(\text{Ti}_{1-x}\text{Mn}_x)_2\text{O}_7$  and  $\text{Sr}_2\text{IrO}_4$  compounds employed in the experimental study of magnetoelectric transitions [2], used for the modeling here.

RP structures have been of interest for solid state physics due to the magnetoresistance effect found in the  $(\text{CaO})-(\text{CaMnO}_3)_n$  ( $n = 1, 2, 3, \infty$ ) compounds [18–21] and high-temperature ferroelectric properties [18,22], which are promising for their potential realization as multiferroics at room temperature [23]. Ferroelectric properties in RP structures emerge due to the rotation of oxygen octahedra [24], which distinguish them from classical perovskite multiferroics, where polarization occurs mainly due to cation displacements. This type of ferroelectricity, referred to as hybrid improper ferroelectricity, was theoretically predicted in double-layered perovskite compounds  $\text{Ca}_3\text{Mn}_2\text{O}_7$  and  $\text{Ca}_3\text{Ti}_2\text{O}_7$  and then detected experimentally in the composites  $\text{Ca}_{3-x}\text{Sr}_x\text{Ti}_2\text{O}_7$  and  $\text{Ca}_3(\text{Ti}_{1-x}\text{Mn}_x)_2\text{O}_7$  [22].

$\text{Ca}_3\text{Mn}_2\text{O}_7$  is antiferromagnet with Neel ordering temperature  $T_N = 115$  K. A neutron diffraction study [20] has confirmed AFM arrangements of G-type or C-type occurring inside a bi-layer plane and weak ferromagnetic state below 100 K. Ferroelectric phase transition in  $\text{Ca}_3\text{Mn}_2\text{O}_7$  is observed near  $T_C = 280$  K and exists up to RT. The crystal structure of  $\text{Ca}_3\text{Mn}_2\text{O}_7$  above room temperature (RT), is described by the tetragonal space group  $I4/mmm$  and at RT by the space group  $Cmc2_1$  [25]. The transition from the  $I4/mmm$  to  $Cmc2_1$  phase occurs through an intermediate phase. Substitution of magnetic ions at the A-positions ( $\text{Ca}_{3-x}\text{La}_x\text{Mn}_2\text{O}_7$ ) or ferroelectric ions in the B-positions ( $\text{Ca}_3(\text{Ti}_{1-x}\text{Mn}_x)_2\text{O}_7$ ) lead to structural transformations, presumably passing through the phases  $I4/mmm \rightarrow Fmmm \rightarrow Cmcm \rightarrow Cmc2_1$  at 200–300 °C [25].

Another representative of the layered perovskites is  $\text{Sr}_2\text{IrO}_4$ , a spin-orbit coupled insulator with weak ferromagnetic properties [12,26]. Although  $\text{Sr}_2\text{IrO}_4$  was synthesized in 1990s [27], interest in the study of transition metal-layered compounds has been renewed due to expectations of superconductive properties [12], non-trivial electronic structure, and manifestation of magnetoelectric properties in superlattices [16]. Polycrystalline  $\text{Sr}_2\text{IrO}_4$  is insulating and shows ferromagnetic ordering in the vicinity of 240 K; the symmetry allowed DMI leads the appearance of weak ferromagnetic properties. The canting angle of magnetic sublattices is about  $8^\circ$  and the magnitude of magnetization emerging due to the canting is about  $0.14 \mu_B$ , which is considered a sufficiently large value [25]. A square lattice of  $\text{Ir}^{4+}$  ions is formed by corner-shared  $\text{IrO}_6$  octahedra, elongated along the c-axis, and rotated about it by  $11^\circ$  [20]. Crystal structure of  $\text{Sr}_2\text{IrO}_4$  is similar to the structures of  $\text{NiF}_4$ , superconductors  $(\text{La,Ba})_2\text{CuO}_4$ , and  $\text{Sr}_2\text{RuO}_4$  [12]. Due to a rotation of the  $\text{IrO}_6$

octahedra about the  $c$  axis, the space-group symmetry is reduced to  $I4_1/acd$  from  $I4/mmm$ . Magnetic interactions and origin of the magnetization in this compound is described in Refs. [12,26]. In our further analysis, we consider the properties of the structure from symmetrical positions.

As in most RP structures, the high-symmetry phase is described by tetragonal  $I4/mmm$  space group; we consider it as the parent phase and apply the symmetry analysis to explore the magnetoelectric properties of the RP structures. In consistence with the data of experimental studies [28], we assume the G-type of AFM ordering. So, as magnetic order parameters, we take the ferromagnetic vector  $M$  and the antiferromagnetic vector  $L$ . As ferroelectric order parameter, we take the vector of ferroelectric polarization  $P$ , and we consider the gradient vector  $\nabla = i \frac{\partial}{\partial x} + j \frac{\partial}{\partial y} + k \frac{\partial}{\partial z}$ , used to describe inhomogeneities, which can also be related to strains and deformations. Classification of the basic order parameters according to the irreducible representation of the space symmetry group is given in Table 1. The decomposition of the basic functions into irreducible representations of the symmetry group  $I4/mmm$  allows one to obtain information on the properties of a system.

**Table 1.** Irreducible representations of the  $I4/mmm$  symmetry group and basic functions.

$\Gamma_i$	$2C_{4z}$	$C_{2z}$	$2C_{2y}$	$\bar{1}$	Basic Vectors $M, L, P, \nabla$
$\Gamma_1$	1	1	1	1	
$\Gamma_2$	1	1	-1	1	$M_z$
$\Gamma_3$	-1	1	-1	1	
$\Gamma_4$	-1	1	1	1	
$\Gamma_5$	$\begin{pmatrix} 0 & 1 \\ -1 & 0 \end{pmatrix}$	$\begin{pmatrix} -1 & 0 \\ 0 & -1 \end{pmatrix}$	$\begin{pmatrix} -1 & 0 \\ 0 & 1 \end{pmatrix}$	$\begin{pmatrix} 1 & 0 \\ 0 & 1 \end{pmatrix}$	$\begin{pmatrix} M_x \\ M_y \end{pmatrix}$
$\Gamma_6$	1	1	1	-1	$L_z$
$\Gamma_7$	1	1	-1	-1	$P_z, \nabla_z$
$\Gamma_8$	-1	1	-1	-1	
$\Gamma_9$	-1	1	1	-1	
$\Gamma_{10}$	$\begin{pmatrix} 0 & 1 \\ -1 & 0 \end{pmatrix}$	$\begin{pmatrix} -1 & 0 \\ 0 & -1 \end{pmatrix}$	$\begin{pmatrix} -1 & 0 \\ 0 & 1 \end{pmatrix}$	$\begin{pmatrix} -1 & 0 \\ 0 & -1 \end{pmatrix}$	$\begin{pmatrix} P_x, \nabla_x \\ P_y, \nabla_y \end{pmatrix}$
$\Gamma'_{10}$	$\begin{pmatrix} 0 & 1 \\ -1 & 0 \end{pmatrix}$	$\begin{pmatrix} -1 & 0 \\ 0 & -1 \end{pmatrix}$	$\begin{pmatrix} 1 & 0 \\ 0 & -1 \end{pmatrix}$	$\begin{pmatrix} -1 & 0 \\ 0 & -1 \end{pmatrix}$	$\begin{pmatrix} L_x \\ L_y \end{pmatrix}$

Using Table 1, one can construct invariant combinations between order parameters ( $M, L, P, \nabla$ ) contributing to the energy of a system. Magnetoelectric contribution is determined by terms  $M_z(P_x L_x + P_y L_y)$ ;  $L_z(M_x P_x + M_y P_y)$ ;  $P_z(M_x L_x + M_y L_y)$ ;  $M_z P_z L_z$ ; the relation between components of ferroelectric polarization vector and magnetic field are determined as

$$P_x = \gamma_3 L_z H_x + \gamma_2 L_x H_z, P_y = \gamma_3 L_z H_y + \gamma_2 L_y H_z, P_z = \gamma_4 (L_x H_x + L_y H_y) + \gamma_5 L_z H_z$$

## 2.2. Dzyaloshinskii–Moriya Interaction and Magnetoelectric Effect

The DMI, also known as antisymmetric spin exchange interaction, occurs in systems whose symmetry group lacks the space inversion symmetry operation. Generally, the DMI energy has the form

$$H_{DMI} = \frac{1}{2} \sum_{i < j} \mathbf{D}_{ij} [\mathbf{S}_i \times \mathbf{S}_j] \quad (1)$$

where  $\mathbf{S}_i, \mathbf{S}_j$  are the spins of neighboring ions,  $\mathbf{D}_{ij} = -\mathbf{D}_{ji}$  is the DM axial vector determined by the Keffer formula [29]:

$$\mathbf{D}_{ij} = V_0 [\mathbf{d} \times \mathbf{r}_{ij}] \quad (2)$$

where  $V_0$  is the microscopic constant,  $\mathbf{r}_{ij}$  is the radius-vector connecting the  $i$ -th and the  $j$ -th ions;  $\mathbf{d}$  is the vector that determines the non-magnetic  $O^{2-}$  ion displacement.

In the beginning of its introduction (1960s), this interaction was employed to explain weak ferromagnetism in two-sublattice canted antiferromagnets such as  $Fe_2O_3$ ,  $MnCO_3$ ,  $MnF_2$ , and  $NiF_2$  [30]. Later on (1990s–2000s), it was found that the DMI can lead to stabilization of the curling and incommensurate magnetic states such as vortices, cycloids, and spirals. In its turn, the presence of inhomogeneous magnetic states results in the emergence of magnetoelectric properties in a system [31].

A striking example, illustrating correlation between DMI and magnetoelectricity, is multiferroic  $BiFeO_3$ . In  $BiFeO_3$ , the DMI manifests itself in two ways: (i) the DMI leads to the canting of magnetic sublattices and (ii) stabilizes the incommensurate antiferromagnetic cycloid acting as magnetoelectric interaction [31].

In 1980–2013, A. Fert and coworkers developed the idea that the DMI should emerge at interfaces due to the large spin-orbit coupling [32,33].

In 2002, A.K. Zvezdin suggested introducing the Lifshitz surface invariant to describe incommensurate structures on surfaces and interfaces [34]. Later, an experiment on the chiral magnetic order of atomic layers of Mn on surfaces  $W(110)$  due to inversion asymmetry was reported in Ref. [35].

Quite recently, the DMI manifested itself in the low-dimensional systems, such as in 2D Janus magnet materials  $MnXY$ :  $MnSeTe$ ,  $MnSTe$ ,  $CrXY$ , and  $Fe_3GeTe_2$  [36]. It can also appear at interfaces due to the Rashba effect [37]. The particular form of the interfacial DMI Hamiltonian is determined by the symmetry of a system. As a consequence, the topology of magnetic inhomogeneities stabilized by the DMI and the manifestations of the magnetoelectric effect in its vicinity also differ depending on the symmetry of the system.

### 2.3. Hamiltonian and Magnetic Ground States

To model the possible magnetic states in a superlattice consisting of antiferromagnetic and ferroelectric sublattices on a triangular lattice with in-plane magnetic anisotropy, we start with the Hamiltonian of the system (See Figure 1), which contains four contributions.

$$H = H_{fm} + H_{fe} + H_{me} + H_{DM} \quad (3)$$

where  $H_{fm}$ -is the Hamiltonian of the frustrated magnetic subsystem with the classical Heisenberg spin.  $H_{fm}$  consists of two parts: the first one is Heisenberg exchange interaction, the second one is Hamiltonian of in-plane magnetic anisotropy,

$$H_{fm} = -J^m \sum_{i,j} \vec{S}_i \cdot \vec{S}_j + K \sum_i \left( S_i^x S_{i+\vec{y}}^x + S_i^y S_{i+\vec{x}}^y \right) \quad (4)$$

where the summation is performed over all nearest neighbors  $S_j$  of the considered spin  $S_i$  at the corresponding lattice nodes  $i$  and  $j$ .  $J^m < 0$  is the integral of antiferromagnetic exchange interaction,  $K$  is the in-plane anisotropy constant,  $\vec{x}$  and  $\vec{y}$  are unit vectors.

$$H_{fe} = -J^e \sum_{i,j} \vec{P}_i \cdot \vec{P}_j \quad (5)$$

$H_{fe}$  is the Hamiltonian of an electrical subsystem; here, the electrical polarization is supposed to be oriented perpendicular to the lattice plane.  $J^e$  determines the interaction between two neighboring polarizations (we suppose  $J^e > 0$ ). The summation is performed over all the nearest polarizations  $P_j$  relative to  $P_i$ .

$$H_{me} = J^{me} \sum_{i,j,k} P_k^z \left( \vec{S}_i \cdot \vec{S}_j \right) \quad (6)$$

$H_{me}$  is the Hamiltonian of the magnetoelectric interaction.  $J^{me}$  is the parameter of the magnetoelectric interaction between the polarization  $P_k$  in the electric layer and the nearest neighboring spin  $S_i$  in the antiferromagnetic layer.

$H_{DM}$  is the Dzyaloshinskii–Moriya Hamiltonian, determined by Equation (1).

Ground states (GSs) of the system have been found numerically by the steepest descent method procedure. To use this method, a triangular lattice of lateral dimension  $L$  has been considered. The total number of sites  $N$  is given by  $N = L \times L$ . The lateral dimensions of the film are taken to be  $L = (40\text{--}400)$ . In the considered model, for simplicity of calculations, the values of exchange coupling parameters are taken to be  $J^m = -1$ ,  $J^e = 1$ .

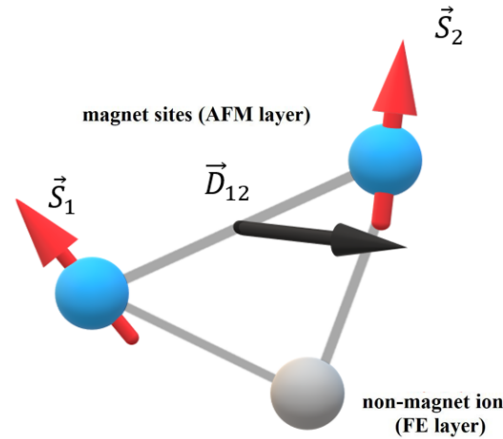


**Figure 1.** Magneto-ferroelectric bi-layer; blue circles represent positions of the spins in the  $xy$  plane, and gray circle correspond to positions of the non-magnetic ion, defining the Dzyaloshinskii–Moriya (DM) vector.

### 3. Results

In this section we present the results of calculations of the ground magnetic states in the superlattice composed of alternately ferroelectric and antiferromagnetic layers with interfacial DMI, the energy of which is described by Equations (1)–(5). Briefly, the main results are listed below:

- The Interfacial DMI leads to stabilization of the skyrmionic structure in the antiferromagnetic-ferroelectric superlattice;
- The skyrmion lattice can be realized in zero magnetic field at a definite combination between the magnetoelectric exchange coupling parameter and the constant of interfacial DMI;
- Three phases—antiferromagnetic phase, skyrmion phase, and the skyrmion lattice phase—have been found in the system under consideration.

Now, let us describe the obtained results in more detail:

1. At first, we calculated the ground magnetic states in the system when magnetic anisotropy and the external magnetic field are absent ( $K = 0$ ,  $H = 0$ ). The results of these calculations are shown in Figure 2. This result shows that the DMI leads to the stabilization of skyrmion-like states. One can see the closely packed skyrmion periodic structure with small local defects stabilized by the interfacial DMI ( $D = 0.5$ ), and the magnetoelectric interaction parameter is taken:  $J^{me} = 2.20$ .
2. Then, we considered the influence of in-plane magnetic anisotropy. Plots illustrating transformations of spin structures at the gradual change of the magnetic anisotropy constant  $K$  are shown in Figure 3. As seen in Figure 3a,b, when the magnetic anisotropy constant changes slightly, the gradual destruction of the skyrmion lattice phase is observed, which is manifested in an increase in the size and distortion of the skyrmion structure. With a further increase in the anisotropy constant (Figure 3c,d), the skyrmion lattice becomes destroyed, and a transition to the antiferromagnetic phase occurs.
3. The phase diagram of the transitions between three phases dependent on the magnetic anisotropy constant is shown in Figure 4. According to the results shown in Figure 4, phase transition from the skyrmion lattice into the skyrmion phase and, afterwards, to

the uniform antiferromagnetic structure can occur even in the absence of an external magnetic field and is regulated by magnetic anisotropy.

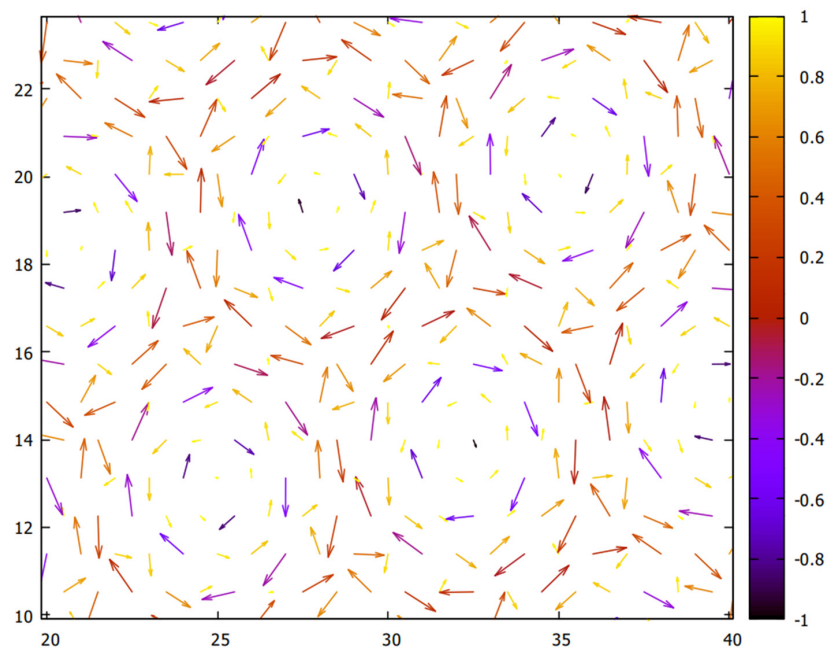


**Figure 2.** Ground state spin configuration of antiferromagnetic layer corresponds to skyrmion state. The parameters of the model (See Equation (1)):  $D = 0.5$ ,  $J^{me} = 2.2$ ,  $J^m = -1$ ,  $J^e = 1$ ,  $K = 0$ .

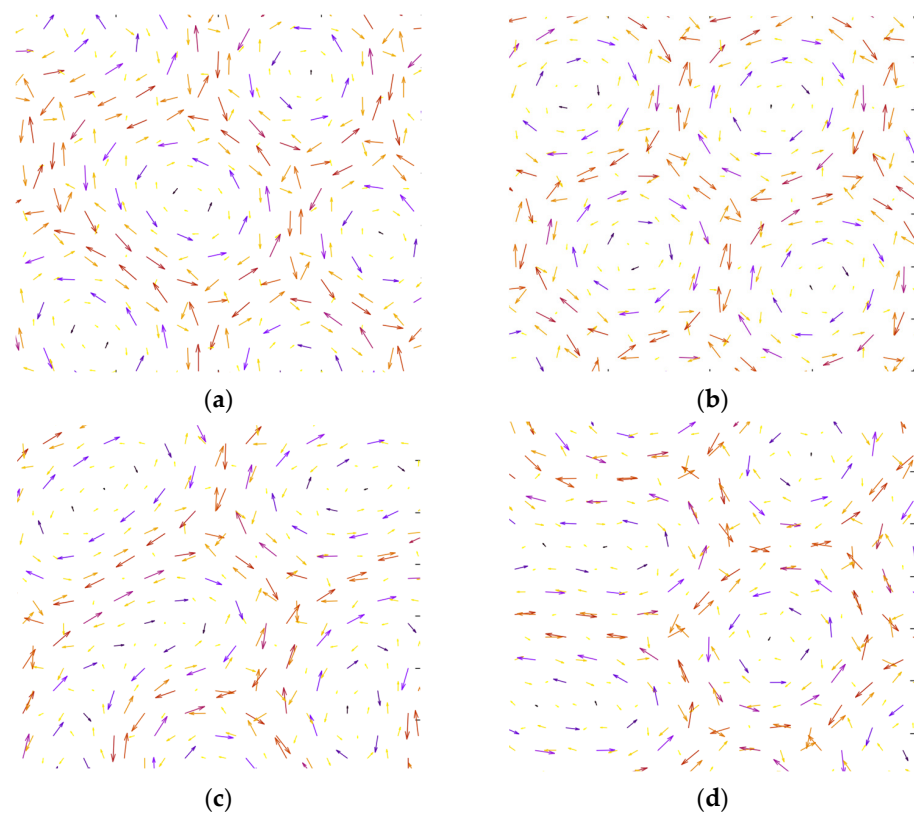


**Figure 3.** Plots illustrating the transformations of the ground state spin configuration of antiferromagnetic layer with skyrmion lattice at different magnetic anisotropy constants. Here  $D = 0.5$ ,  $J^{me} = 2.2$ ,  $J^m = -1.0$ ,  $J^e = 1.0$ . (a)  $K = 0.1$ ; (b)  $K = 0.2$ ; (c)  $K = 0.45$ ; (d)  $K = 0.48$ . Vectors with blue color correspond to spins with  $S^z < 0$ ; vectors with red color correspond to spins with  $S^z > 0$ .

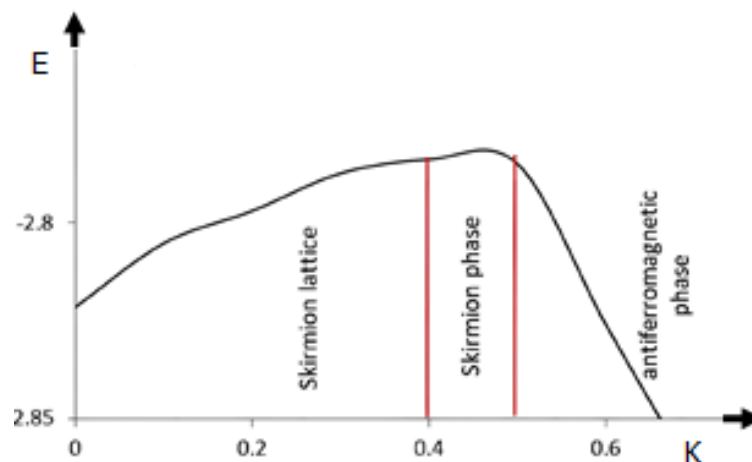


**Figure 4.** Dependence of the ground state energy versus the value of magnetic anisotropy constant. The parameters of the model (See Equation (1)):  $D = 0.5$ ,  $J^{me} = 2.2$ ,  $J^m = -1$ ,  $J^e = 1$ .

We calculated the value of the ground state by using the steepest descent method. This numerical approach consists of minimizing the energy of each spin in the antiferromagnetic film (or polarization in the ferroelectric layer) of the bilayer by aligning it parallel to the local field acting on every lattice site from its nearest neighbors.

When  $K \in (0.0, 0.45)$ , the ground state energy increases with  $K$ . The phase of the skyrmion lattice has the lowest energy in the absence of anisotropy. As parameter  $K$  increases, an SkL phase goes into the phase with randomly distributed skyrmions, becoming the ground state at  $K \in (0.45, 0.48)$ . (See Figure 3c, where one can see that some of the skyrmions on the left side of Figure 3c,d lose their texture and actually turn into a domain with a noncollinear spin distribution.) This phase has randomly distributed skyrmions that remain energetically more favorable (than SkL phase) even at  $K = 0.5$ .

As  $K$  increases above 0.48, the skyrmions are suppressed, and the antiferromagnetic state (red area) has the lowest energy, even at large  $D$ .

The phase diagram of states in  $J^{mf} - K$  plane at the characteristic value of the Dzyaloshinskii–Moriya plane vector parameter  $D = 0.5$  is shown in Figure 5. Stabilization of the nanosized topological protected structures, such as skyrmions, is a key challenge for new technological devices. The compass-type anisotropy plays a crucial role in stabilizing the phase of the skyrmion lattice, and magnetoelectric coupling with frustration (meaning a geometrically frustrated triangular lattice) also strongly affects the stability of the skyrmions.

Note that strong in-plane anisotropy suppresses the skyrmion structure and a region with magnetic inhomogeneities is formed, which does not contain structures with a nonzero topological charge. There exists a threshold value in  $K$  above which skyrmion becomes metastable.

In our case, this is accompanied by an increase in the linear size of the skyrmion; at a threshold value of the anisotropy ( $K = 0.4$ ), the skyrmion transforms into a region with magnetic inhomogeneity, and, if the parameter of the magnetoelectric interaction is large enough, then the inhomogeneity obtains a non-zero topological charge. However, this inhomogeneity is not a skyrmion. With a large  $K$  ( $K = 0.3$ ), the spatial profile—the spatial modulation—becomes largely anisotropy-dependent, and the magnetization configuration varies from skyrmion to skyrmion with a metastable state.

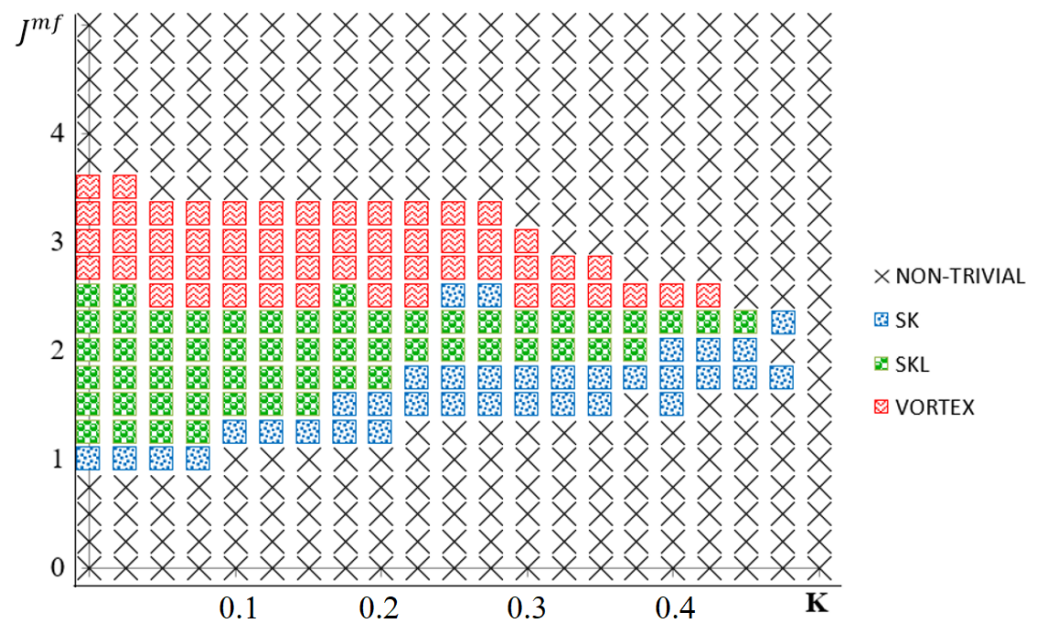


**Figure 5.** Phase diagram of ground states in  $J^{mf} - K$  plane. Green squares (1) correspond to the skyrmion lattice phase, blue color (2) corresponds to randomly distributed skyrmions, red squares correspond to phase with spin vortices, and  $\times$ -labeled area corresponds to ground state configurations that have antiferromagnetic and noncollinear domains.

#### 4. Discussion and Conclusions

Thus, we considered magnetoelectric effect and micromagnetic structures in the perovskite-like superlattices with an interfacial DMI. As the prototype, we have taken the system consisting of antiferromagnetic–ferroelectric (AFM-FE) sublayers with Ruddlesden-Popper structure as the AFM component and ferroelectric perovskite as the FE component. Quite recently, the magnetoelectric effect has been experimentally discovered in such systems, as Ref. [16] reports. It has been shown there that in  $\text{Sr}_2\text{IrO}_4/\text{SrTiO}_3$ , artificially designed ferroelectricity makes it possible to achieve a magnetoelectric state and control it by interfacial DMI. Authors of Ref. [16] explored the transitions to the magnetoelectric phase dependent on the temperatures related to the engineered interfacial DMI, and they determined the presence of the required state using the data on ferroelectric polarization.

In this paper, we perform theoretical analysis of the conjugate system with  $C_{nv}$  symmetry. Our analysis shows that three types of magnetic ordering—(i) uniform antiferromagnetic state, (ii) skyrmion state, (iii) skyrmion lattice state—are realized in this structure at the definite relation between intrinsic system parameters: the constants of magnetic anisotropy, the interfacial DMI, and the magnetoelectric exchange interaction.

As known, topological structures with non-uniform distribution of spins, such as skyrmions, vortices, and domain walls, play an important role in manifestations of magnetoelectricity. In consistence with the concept of inhomogeneous magnetoelectric effect [38], the ferroelectric polarization emerging close to magnetic inhomogeneity is determined through the gradients of magnetization vectors:

$$\mathbf{P} = \gamma\chi_e[(\mathbf{M} \cdot \nabla)\mathbf{M} - \mathbf{M}(\nabla \cdot \mathbf{M})] \quad (7)$$

where  $\mathbf{M}$  is the magnetization,  $\mathbf{P}$  is the polarization,  $\chi_e$  is electric susceptibility, and  $\gamma$  is the coefficient of ME effect.

Polarization induced by magnetic inhomogeneity can be controlled using a magnetic field, including that created by an electric current. Figure 6 shows how the polarization value changes in a nanosized magnetic film with interfacial DMI during magnetization and remagnetization reversal. In Figure 6, we show the results of simulations conducted with the use of the OOMMF package [39] for the iron garnet film with a thickness 30 nm and

transverse dimensions  $200 \times 200$  nm,  $D = 0.2$  mJ/m<sup>2</sup>, here, in a zero magnetic field, the ground magnetic state is vortex structure (see inset in Figure 6).

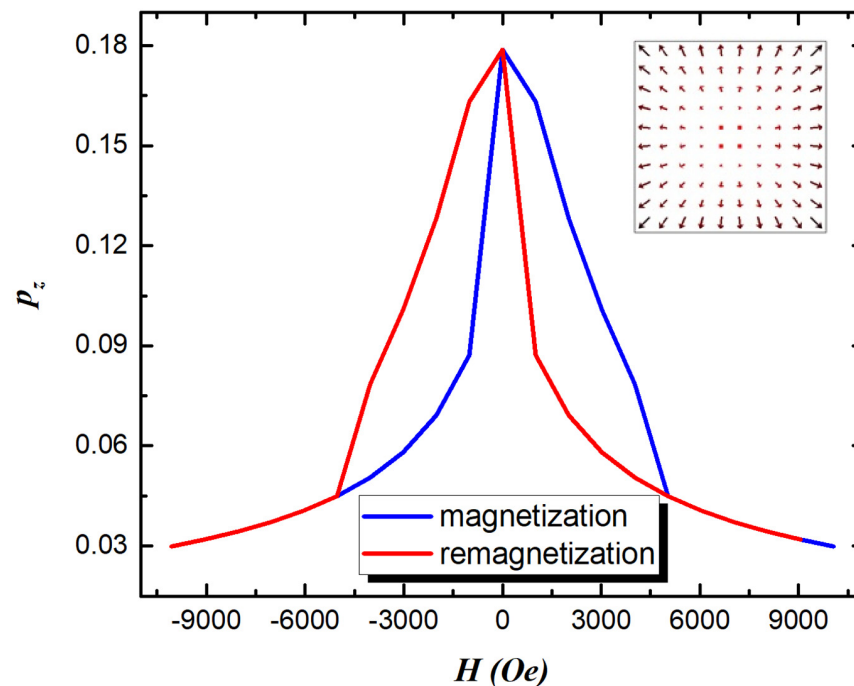


**Figure 6.** Dependence of the reduced  $p_z$ -component of electric polarization on magnetic field in nanosized ferromagnetic film with interface DMI,  $D = 0.2$  mJ/m<sup>2</sup>; thickness of film is 30 nm; the lateral dimensions are  $200 \times 200$  nm.  $p_z = P_z/\gamma\chi_e$ , inset—magnetic vortex at  $H = 0$ .

Thus, if desired, the given analysis can be represented in terms of polarization, which should show the emergence of a magnetoelectric phase in states with inhomogeneous skyrmionics-like structures. So far, we highlight this issue as a direction for future research.

Our present study aimed to point out a novel possibility of realizing the magnetoelectric effect in two-dimensional perovskite multiferroics. We justified the existence of magnetoelectric states in the multiferroic perovskite superlattice structure with interfacial DMI using the group-theoretical approach in combination with micromagnetic simulations. Based on the analysis of irreducible representations of the symmetry of the top AFM layer, we determined the actual order parameters for the RP structures, possible couplings, and invariant contributions to the energy. The ground magnetic states of the system have been calculated by minimizing the energy with the use of a fast steepest descent method for the frustrated antiferromagnetic Heisenberg triangular lattice including a DMI with an in-plane DM vector.

The controlled ME effect implies its great potential for the development of the functionality of integrated magnetoelectronic superlattices. The research in this direction will advance the understanding of coupling mechanisms in multiferroic superlattices and their potential applications in spintronic technologies.

**Author Contributions:** All co-authors, Z.G., I.S. and A.Z., made an equal contribution to the conceptualization, methodology, validation, formal analysis, investigation, writing—original draft preparation, and writing—review and editing of the present manuscript. All authors have read and agreed to the published version of the manuscript.

**Funding:** Z. Gareeva acknowledges the support by Russian Science Foundation No. 23-22-00225, I. Sharafullin acknowledges the support by the State assignment for the implementation of scientific research by laboratories (Order MN-8/1356 of 09/20/2021), and A. Zvezdin acknowledges the support by Ministry of Science and Higher Education of the Russian Federation, Agreement No. 075-11-2022-046.

**Data Availability Statement:** Not applicable.

**Conflicts of Interest:** The authors declare no conflict of interest.

## References

1. Hu, J.-M.; Duan, C.-G.; Nan, C.-W.; Chen, L.-Q. Understanding and Designing Magnetoelectric Heterostructures Guided by Computation: Progresses, Remaining Questions, and Perspectives. *Npj Comput. Mater.* **2017**, *3*, 1.
2. Meisenheimer, P.B.; Novakov, S.; Vu, N.M.; Heron, J.T. Perspective: Magnetoelectric Switching in Thin Film Multiferroic Heterostructures. *J. Appl. Phys.* **2018**, *123*, 240901. [[CrossRef](#)]
3. Trier, F.; Noël, P.; Kim, J.-V.; Attané, J.-P.; Vila, L.; Bibes, M. Oxide Spin-Orbitronics: Spin-Charge Interconversion and Topological Spin Textures. *Nat. Rev. Mater.* **2022**, *7*, 4. [[CrossRef](#)]
4. Hwang, H.Y.; Iwasa, Y.; Kawasaki, M.; Keimer, B.; Nagaosa, N.; Tokura, Y. Emergent Phenomena at Oxide Interfaces. *Nat. Mater.* **2012**, *11*, 2. [[CrossRef](#)]
5. Katsura, H.; Nagaosa, N.; Balatsky, A.V. Spin Current and Magnetoelectric Effect in Noncollinear Magnets. *Phys. Rev. Lett.* **2005**, *95*, 057205. [[CrossRef](#)]
6. Sergienko, I.A.; Dagotto, E. Role of the Dzyaloshinskii-Moriya Interaction in Multiferroic Perovskites. *Phys. Rev. B* **2006**, *73*, 094434. [[CrossRef](#)]
7. Pyatakov, A.P.; Gareev, T.T.; Kaminskiy, A.S.; Antipin, K.S.; Nikolaeva, E.P.; Kulikova, D.P.; Sergeev, A.S.; Nikolaev, A.V. Magnetoelectricity of Chiral Micromagnetic Structures. In *Chirality, Magnetism and Magnetoelectricity: Separate Phenomena and Joint Effects in Metamaterial Structures*; Kamenetskii, E., Ed.; Springer International Publishing: Cham, Switzerland, 2021; pp. 127–146.
8. Eglitis, R.I.; Bocharov, D.; Piskunov, S.; Jia, R. Review of First Principles Simulations of STO/BTO, STO/PTO, and SZO/PZO (001) Heterostructures. *Crystals* **2023**, *13*, 799. [[CrossRef](#)]
9. Eglitis, R.I.; Piskunov, S.; Popov, A.I.; Purans, J.; Bocharov, D.; Jia, R. Systematic Trends in Hybrid-DFT Computations of BaTiO<sub>3</sub>/SrTiO<sub>3</sub>, PbTiO<sub>3</sub>/SrTiO<sub>3</sub> and PbZrO<sub>3</sub>/SrZrO<sub>3</sub> (001) Hetero Structures. *Condens. Matter.* **2022**, *7*, 70. [[CrossRef](#)]
10. Matsuno, J.; Ogawa, N.; Yasuda, K.; Kagawa, F.; Koshibae, W.; Nagaosa, N.; Tokura, Y.; Kawasaki, M. Interface-Driven Topological Hall Effect in SrRuO<sub>3</sub>-SrIrO<sub>3</sub> Bilayer. *Sci. Adv.* **2016**, *2*, e1600304. [[CrossRef](#)]
11. Yang, L.; Wysocki, L.; Schöpfl, J.; Jin, L.; Kovács, A.; Gunkel, F.; Dittmann, R.; van Loosdrecht, P.H.M.; Lindfors-Vrejoiu, I. Origin of the Hump Anomalies in the Hall Resistance Loops of Ultrathin SrRuO<sub>3</sub>/SrIrO<sub>3</sub> Multilayers. *Phys. Rev. Mater.* **2021**, *5*, 014403. [[CrossRef](#)]
12. Cao, G.; Bolivar, J.; McCall, S.; Crow, J.E.; Guertin, R.P. Weak Ferromagnetism, Metal-to-Nonmetal Transition, and Negative Differential Resistivity in Single-Crystal Sr<sub>2</sub>IrO<sub>4</sub>. *Phys. Rev. B* **1998**, *57*, R11039. [[CrossRef](#)]
13. Ma, X.; Yu, G.; Razavi, S.A.; Sasaki, S.S.; Li, X.; Hao, K.; Tolbert, S.H.; Wang, K.L.; Li, X. Dzyaloshinskii-Moriya Interaction across an Antiferromagnet-Ferromagnet Interface. *Phys. Rev. Lett.* **2017**, *119*, 027202. [[CrossRef](#)] [[PubMed](#)]
14. Wang, H.; Dai, Y.; Liu, Z.; Xie, Q.; Liu, C.; Lin, W.; Liu, L.; Yang, P.; Wang, J.; Venkatesan, T.V.; et al. Overcoming the Limits of the Interfacial Dzyaloshinskii-Moriya Interaction by Antiferromagnetic Order in Multiferroic Heterostructures. *Adv. Mater.* **2020**, *32*, 1904415. [[CrossRef](#)] [[PubMed](#)]
15. Skoropata, E.; Nichols, J.; Ok, J.M.; Chopdekar, R.V.; Choi, E.S.; Rastogi, A.; Sohn, C.; Gao, X.; Yoon, S.; Farmer, T.; et al. Interfacial tuning of chiral magnetic interactions for large topological Hall effects in LaMnO<sub>3</sub>/SrIrO<sub>3</sub> heterostructures. *Sci. Adv.* **2020**, *6*, 3902. [[CrossRef](#)] [[PubMed](#)]
16. Liu, X.; Song, W.; Wu, M.; Yang, Y.; Yang, Y.; Lu, P.; Tian, Y.; Sun, Y.; Lu, J.; Wang, J.; et al. Magnetoelectric Phase Transition Driven by Interfacial-Engineered Dzyaloshinskii-Moriya Interaction. *Nat. Commun.* **2021**, *12*, 1. [[CrossRef](#)]
17. Urru, A.; Ricci, F.; Filippetti, A.; Íñiguez, J.; Fiorentini, V. A Three-Order-Parameter Bistable Magnetoelectric Multiferroic Metal. *Nat. Commun.* **2020**, *11*, 1. [[CrossRef](#)]
18. Oh, Y.S.; Luo, X.; Huang, F.-T.; Wang, Y.; Cheong, S.-W. Experimental Demonstration of Hybrid Improper Ferroelectricity and the Presence of Abundant Charged Walls in (Ca,Sr)<sub>3</sub>Ti<sub>2</sub>O<sub>7</sub> Crystals. *Nat. Mater.* **2015**, *14*, 407. [[CrossRef](#)]
19. Battle, P.D.; Rosseinsky, M.J. Synthesis, Structure, and Magnetic Properties of N = 2 Ruddlesden-Popper Manganates. *Curr. Opin. Solid State Mater. Sci.* **1999**, *4*, 163. [[CrossRef](#)]
20. Harris, A.B. Symmetry Analysis for the Ruddlesden-Popper Systems Ca<sub>3</sub>Mn<sub>2</sub>O<sub>7</sub> and Ca<sub>3</sub>Ti<sub>2</sub>O<sub>7</sub>. *Phys. Rev. B* **2011**, *84*, 064116. [[CrossRef](#)]
21. Lobanov, M.V.; Greenblatt, M.; Caspi, E.A.N.; Jorgensen, J.D.; Sheptyakov, D.V.; Toby, B.H.; Botez, C.E.; Stephens, P.W. Crystal and Magnetic Structure of the Ca<sub>3</sub>Mn<sub>2</sub>O<sub>7</sub> Ruddlesden-Popper Phase: Neutron and Synchrotron X-ray Diffraction Study. *J. Condens. Matter Phys.* **2004**, *16*, 5339. [[CrossRef](#)]
22. Liu, X.Q.; Wu, J.W.; Shi, X.X.; Zhao, H.J.; Zhou, H.Y.; Qiu, R.H.; Zhang, W.Q.; Chen, X.M. Hybrid Improper Ferroelectricity in Ruddlesden-Popper Ca<sub>3</sub>(Ti,Mn)<sub>2</sub>O<sub>7</sub> Ceramics. *Appl. Phys. Lett.* **2015**, *106*, 202903. [[CrossRef](#)]
23. Zhang, B.H.; Liu, X.Q.; Chen, X.M. Review of Experimental Progress of Hybrid Improper Ferroelectricity in Layered Perovskite Oxides. *J. Phys. D Appl. Phys.* **2021**, *55*, 113001. [[CrossRef](#)]
24. Benedek, N.A.; Fennie, C.J. Hybrid Improper Ferroelectricity: A Mechanism for Controllable Polarization-Magnetization Coupling. *Phys. Rev. Lett.* **2011**, *106*, 107204. [[CrossRef](#)] [[PubMed](#)]

25. Bendersky, L.A.; Chen, R.; Fawcett, I.D.; Greenblatt, M. TEM Study of the Electron-Doped Layered  $\text{La}_{2-2x}\text{Ca}_{1+2x}\text{Mn}_2\text{O}_7$ : Orthorhombic Phase in the 0.8. *J. Solid State Chem.* **2001**, *157*, 309. [[CrossRef](#)]
26. Jackeli, G.; Khaliullin, G. Mott Insulators in the Strong Spin-Orbit Coupling Limit: From Heisenberg to a Quantum Compass and Kitaev Models. *Phys. Rev. Lett.* **2009**, *102*, 017205. [[CrossRef](#)]
27. Huang, Q.; Soubeyroux, J.L.; Chmaissem, O.; Sora, I.N.; Santoro, A.; Cava, R.J.; Krajewski, J.J.; Peck, W.F. Neutron Powder Diffraction Study of the Crystal Structures of  $\text{Sr}_2\text{RuO}_4$  and  $\text{Sr}_2\text{IrO}_4$  at Room Temperature and at 10 K. *J. Solid State Chem.* **1994**, *112*, 355. [[CrossRef](#)]
28. Guiblin, N.; Grebille, D.; Leligny, H.; Martin, C.  $\text{Ca}_3\text{Mn}_2\text{O}_7$ . *Acta Cryst. C* **2002**, *58*, 1. [[CrossRef](#)]
29. Keffer, F. Moriya Interaction and the Problem of the Spin Arrangements in  $\beta\text{MnS}$ . *Phys. Rev.* **1962**, *126*, 896. [[CrossRef](#)]
30. Galkina, E.G.; Kulagin, N.E.; Ivanov, B.A. Dynamics of Dzyaloshinskii Domain Walls for Ferrimagnets with Compensation of Angular Momentum. *Ann. Phys.* **2022**, *447*, 169080. [[CrossRef](#)]
31. Zvezdin, A.K.; Pyatakov, A.P. On the Problem of Coexistence of the Weak Ferromagnetism and the Spin Flexoelectricity in Multiferroic Bismuth Ferrite. *EPL* **2012**, *99*, 57003. [[CrossRef](#)]
32. Fert, A.; Cros, V.; Sampaio, J. Skyrmions on the Track. *Nat. Nanotech.* **2013**, *8*, 152. [[CrossRef](#)] [[PubMed](#)]
33. Fert, A.; Levy, P.M. Role of Anisotropic Exchange Interactions in Determining the Properties of Spin-Glasses. *Phys. Rev. Lett.* **1980**, *44*, 1538. [[CrossRef](#)]
34. Zvezdin, A.K. Lifshitz Surface Invariant and Space Modulated Structures in Thin Films. *Bull. Lebedev Phys. Inst.* **2002**, *4*, 7.
35. Bode, M.; Heide, M.; von Bergmann, K.; Ferriani, P.; Heinze, S.; Bihlmayer, G.; Kubetzka, A.; Pietzsch, O.; Blügel, S.; Wiesendanger, R. Chiral Magnetic Order at Surfaces Driven by Inversion Asymmetry. *Nature* **2007**, *447*, 7141. [[CrossRef](#)] [[PubMed](#)]
36. Lu, A.-Y.; Zhu, H.; Xiao, J.; Chuu, C.-P.; Han, Y.; Chiu, M.-H.; Cheng, C.-C.; Yang, C.-W.; Wei, K.-H.; Yang, Y.; et al. Janus Monolayers of Transition Metal Dichalcogenides. *Nat. Nanotech.* **2017**, *12*, 8. [[CrossRef](#)]
37. Yang, H.; Chen, G.; Cotta, A.A.C.; N'diaye, A.T.; Nikolaev, S.A.; Soares, E.A.; Macedo, W.A.A.; Liu, K.; Schmid, A.K.; Fert, A.; et al. Significant Dzyaloshinskii–Moriya Interaction at Graphene–Ferromagnet Interfaces Due to the Rashba Effect. *Nat. Mater.* **2018**, *17*, 7. [[CrossRef](#)]
38. Zvezdin, A.K.; Pyatakov, A.P. Inhomogeneous magnetoelectric interaction in multiferroics and related new physical effects. *Physics-Uspokhi* **2009**, *52*, 845–851. [[CrossRef](#)]
39. Donahue, M.J.; Porter, D.G. *OOMMF User's Guide, Version 1.0*; Interagency Report NISTIR 6376; National Institute of Standards and Technology: Gaithersburg, MD, USA, 1999.

**Disclaimer/Publisher's Note:** The statements, opinions and data contained in all publications are solely those of the individual author(s) and contributor(s) and not of MDPI and/or the editor(s). MDPI and/or the editor(s) disclaim responsibility for any injury to people or property resulting from any ideas, methods, instructions or products referred to in the content.